Supporting information for

Critical Role of Surface Energy in Guiding Crystallization of Solution Coated Conjugated Polymer Thin Films

Fengjiao Zhang[1#], Erfan Mohammadi[1#], Joseph Strzalka[2], Xuyi Luo[3], Jianguo Mei[3], Ying Diao[1*]

[1]*Department of Chemical and Biomolecular Engineering, University of Illinois at Urbana−Champaign, 600 South Mathews Avenue, Urbana, Illinois 61801, United States.*

[2]*X-ray Science Division, Advanced Photon Source, Argonne National Laboratory, Argonne, IL 60349, United States.*

[3]*Department of Chemistry, Purdue University, 560 Oval Drive, West Lafayette, Indiana 47907, United States.*

Downloaded from pubs.acs.org/langd5/article-supplement/1470601/pdf/la7b02807_si_001/ by PURDUE UNIV user on 28 October 2026

Supplementary Note: Substrate Surface Energy Determination

Based on the Young's Equation[1], the contact angle of a pure liquid droplet on a smooth and chemically homogenous solid surface at thermodynamic equilibrium is defined as the balance of three interfacial tensions (Figure S1 and Equation S1):

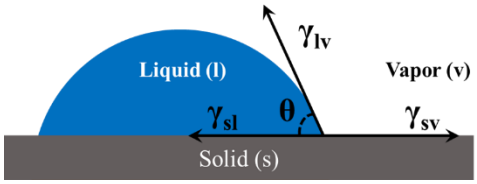

Figure S1. Contact angle at the three-phase contact line.

$$\gamma_{sv} = \gamma_{sl} + \gamma_{lv}cos\theta \qquad \text{(S1)}$$

where γ_{lv}, γ_{sl} and γ_{sv} are liquid-vapor, solid-liquid and solid-vapor interfacial free energies respectively, and θ is the static contact angle (often quasi-static advancing contact angle is used[2]). Liquid-air interfacial free energy of the pure probing liquid (γ_{lv}) and contact angle (θ) can be measured using the pendant and sessile drop methods and axisymmetric drop shape analysis using standard Goniometers.[3] However, one equation is insufficient for determining two unknowns, γ_{sv} and γ_{sl}. It has been shown experimentally that γ_{sv}, γ_{sl} and γ_{lv} are not independent states of the system, but are related via an equation of state[4-6]. In other words, γ_{sl} can be fully determined by γ_{lv} and γ_{sv} (assuming the system is in thermodynamic equilibrium)[2, 4]:

$$\gamma_{sl} = f(\gamma_{sv}, \gamma_{lv}) \qquad \text{(S2)}$$

Specifically, we employ the following equation-of-state relation[2, 7] in our work:

$$\gamma_{sl} = \gamma_{lv} + \gamma_{sv} - 2\sqrt{\gamma_{lv}\gamma_{sv}}(1 - \beta(\gamma_{lv} - \gamma_{sv})^2) \qquad \text{(S3)}$$

Downloaded from pubs.acs.org/langd5/article-supplement/1470601/pdf/la7b02807_si_001/ by PURDUE UNIV user on 28 October 2026

where β is an empirical constant. The $(\gamma_{lv} + \gamma_{sv} - 2\sqrt{\gamma_{lv}\gamma_{sv}})$ term comes from the geometric mean combining rule, which is rooted in London theory of dispersion and assumes one dominant type of interactions between the liquid and the solid molecules, or like pairs[8]. However, the combining rule overestimates the interaction between two dissimilar pairs (unlike pairs) and an empirical parameter ($1-\beta(\gamma_{lv}-\gamma_{sv})^2$) is added to correct for this deviation from experimental results, while maintaining the symmetry of combining rules.[2] By combining Equation S3 with the Young's equation (Equation S1), $\cos\theta$ can be expressed as,

$$\cos\theta = -1 + 2\sqrt{\frac{\gamma_{sv}}{\gamma_{lv}}}(1 - \beta(\gamma_{lv} - \gamma_{sv})^2) \qquad \text{(S4)}$$

By measuring contact angles (θ) with a series of probing liquids with known but diverse surface energies (γ_{lv}), substrate surface energy (γ_{sv}) and β specific for each substrate can be calculated using the least squares regression method.[9] Table S1 summarizes eleven probing liquids selected in this work (chemically inert with respect to substrates within the time frame of contact angle measurements), containing a diverse range of chemistries, intermolecular forces and surface energies (measured in this work or taken from external references).

Table S1. Probing liquids and their surface tensions at ambient temperature.

Probing Liquid	**Surface Tension (mN/m)**	**Reference**
Dodecane	25.4±0.2	[10]
1-Penthanol	26.0	[11]
Hexadecane	27.6	[11]
1-Ethyl-3-methylimidazolium bis(trifluoromethylsulfonyl)imide ([EMIM][TFSI])	36.9 ±0.7	This work
Dimethyl sulfoxide	44.0±1.5	This work

Downloaded from pubs.acs.org/langd5/article-supplement/1470601/pdf/la7b02807_si_001/ by PURDUE UNIV user on 28 October 2026

		and [11]
Ethylene glycol	47.7±0.7	This work and [11]
Diiodomethane	50.0	[11]
Formamide	59.1	[11]
Glycerol	65.0	[11]
Water	72.7	[11]
Mercury	470	[11]

The measurement of θ in the Young's equation is crucial; in accurate θ measurements or the choice of the wrong type of θ (advancing vs. receding, static vs. dynamic) can lead to erroneous results. It has been shown that the quasi-static advancing contact angle, θ_a, is the best approximation to the thermodynamic equilibrium static contact angle[12], which was carefully measured in this study by slowly supplying excess liquid to the sessile drop (the three-phase contact line will move outward during this process). The final volume of the drop was set to be less than 3 μL to avoid the deformation of drop shape by gravitational force. A Rame-Hart Model 250 Standard Goniometer equipped with drop shape analysis software was employed in this work for measuring the contact angles. For each probing liquid and substrate pair, at least 10 different advancing contact angles were collected on new surfaces making sure that the substrates are chemically homogenous and our results are reproducible. The average advancing contact angles thus measured are summarized in Table S2.

Table S2. Advancing contact angles of the probing liquids on various substrates.

	OTS	FPTS	PTS	PVPHDA	Bare	Plasma
Dodecane	32.9±0.3	-	-	-	-	-
1-Penthanol	37.1±0.2	-	-	-	-	-
Hexadecane	41.1±0.2	-	-	-	-	-
[EMIM][TFSI]	75.1±0.5	31.0±0.5	-	-	-	-
Dimethyl	74.3±0.8	43.2±2.0	29.7±0.9	-	-	-

Downloaded from pubs.acs.org/langd5/article-supplement/1470601/pdf/la7b02807_si_001/ by PURDUE UNIV user on 28 October 2026

sulfoxide						
Ethylene glycol	85.4±0.4	62.3±0.3	54.1±0.6	-	-	-
Diiodomethane	76.2±0.7	61.0±0.3	46.7±0.7	35.6±1.7	-	-
Formamide	86.4±1.8	65.9±0.1	59.9±0.9	-	27.1±0.2	-
Glycerol	97.1±0.6	82.0±0.4	74.1±0.6	53.7±2.5	43.4±2.2	12.4±2.3
Water	112.3±0.3	91.1±0.7	80.2±1.5	63.2±3.8	52.0±0.7	9.9±1.7
Mercury	-	-	-	-	-	128.0±1.1

Note that γ_{lv} of the probing liquids usually need to be higher than the solid surface energy γ_{sv} to avoid total wetting conditions (θ=0), under which the Young's equation is no longer valid. Strictly, the total wetting condition is when $\gamma_{lv} + \gamma_{sl} < \gamma_{sv}$, determined by the spreading coefficient. But when $\gamma_{lv} < \gamma_{sv}$, the contact angle can be too small to measure accurately.

Downloaded from pubs.acs.org/langd5/article-supplement/1470601/pdf/la7b02807_si_001/ by PURDUE UNIV user on 28 October 2026

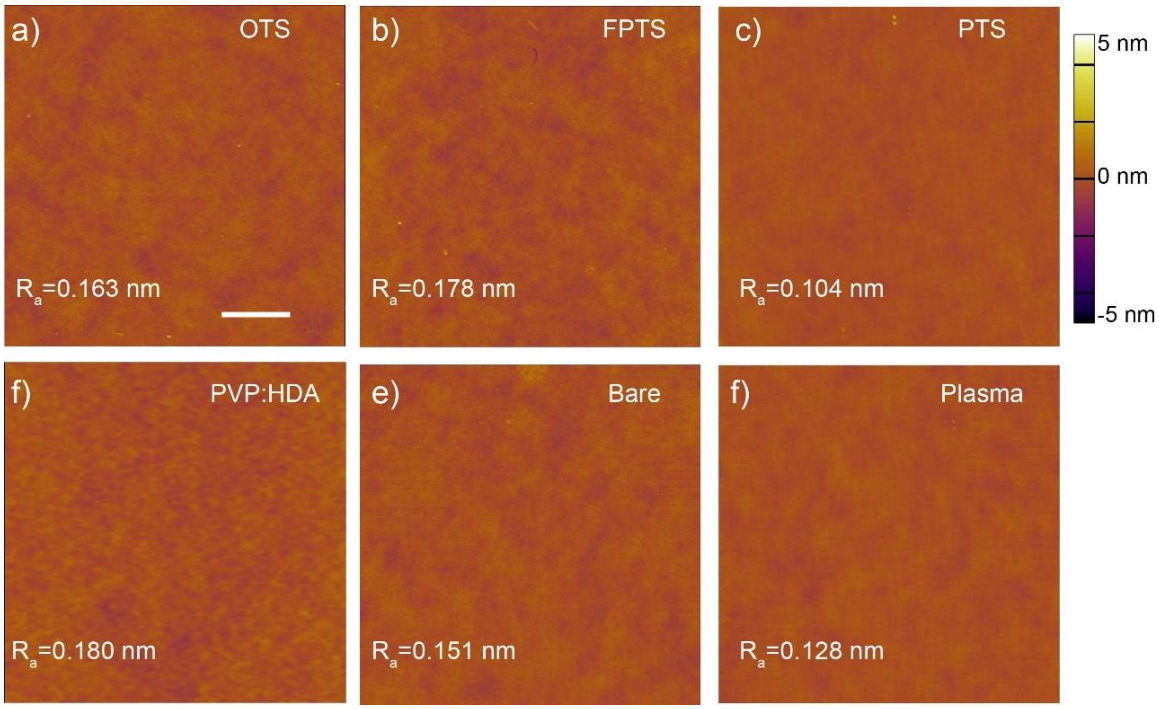

Figure S2. AFM images of the top-surface morphology for (a) OTS, (b) FPTS, (c) PTS, (d) PVP:HDA, (e) bare and (d) plasma treated SiO_2 surface. The scale bare is 1 μm. The mean roughness (R_a) is labeled on the lower left of each image.

Downloaded from pubs.acs.org/langd5/article-supplement/1470601/pdf/la7b02807_si_001/ by PURDUE UNIV user on 28 October 2026

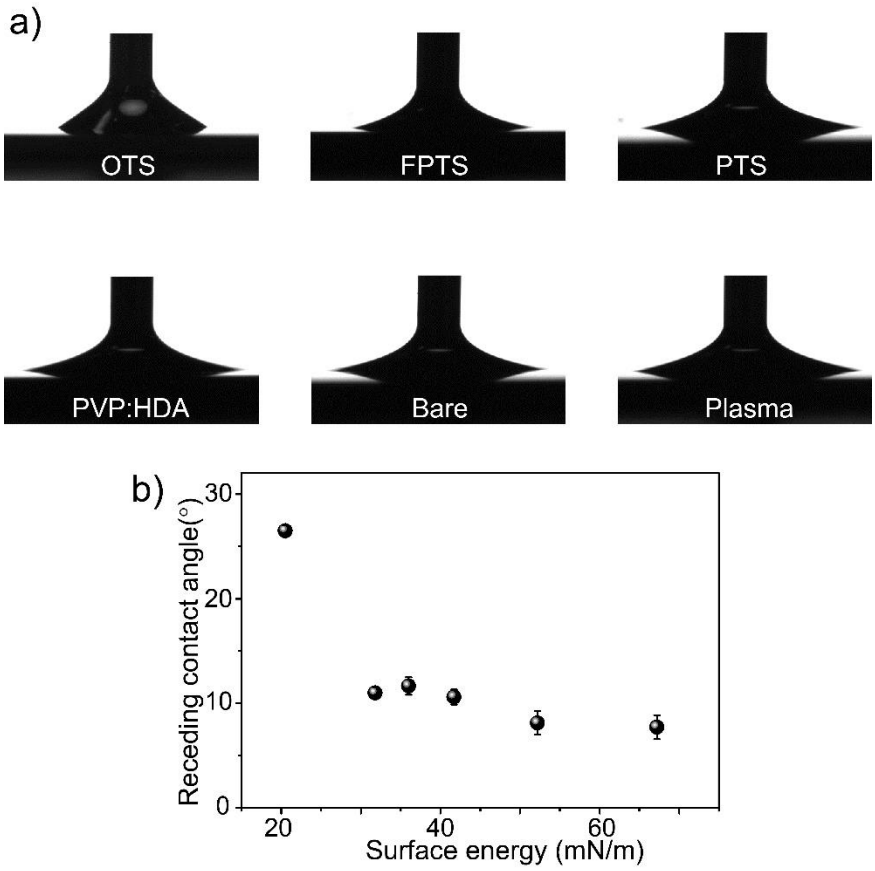

Figure S3. Receding contact angles of chloroform on various substrates. (a) Optical images of receding meniscus of chloroform on various substrates. (b) Receding contact angle as a function of substrate surface energy. The receding contact angles of chloroform on different substrates, which approximate the dynamic contact angle during meniscus-guided coating, were measured during solvent evaporation at room temperature. The receding contact angles for all surfaces fall within a narrow range of 15° and only OTS substrate has a relatively higher value possibly due to the crystalline nature of the OTS SAM as well as the non-polarity imparted by the alkyl chains. Therefore, the meniscus shape for DPP2T-TT/chloroform solution and evaporation rates are comparable for most of the substrates except for OTS. In cases with comparable evaporation rates and wetting properties, the OSC film morphology differed drastically. For instance, even

Downloaded from pubs.acs.org/langd5/article-supplement/1470601/pdf/la7b02807_si_001/ by PURDUE UNIV user on 28 October 2026

though the receding contact angle is similar for chloroform on PTS and PVP:HDA, the degree of crystallinity dramatically decreased comparing films on PTS vs. PVP:HDA. This result validates that the surface energy primarily impacts polymer crystallization, not the ink wetting and drying behaviors. In addition, solvent evaporation rate (Q_{evap}) in meniscus-guided coating configuration can be described from the evaporation regime model by Le Berre et. al. derived from mass balance equation[13]: $Q_{evap}=h\,\rho Lv/C$; where h is the film thickness, ρ is the solute density, L is the meniscus width, ν is the coating speed and C is the solution concentration. We controlled polymer film thickness to be ~30 nm across all substrates by slightly changing concentration within the narrow range of 3.8±0.5 mg/mL for accurate comparison of UV-vis, C-POM and GIXD data. Therefore, Q_{evap} should be comparable across substrates based on the equation above.

Downloaded from pubs.acs.org/langd5/article-supplement/1470601/pdf/la7b02807_si_001/ by PURDUE UNIV user on 28 October 2026

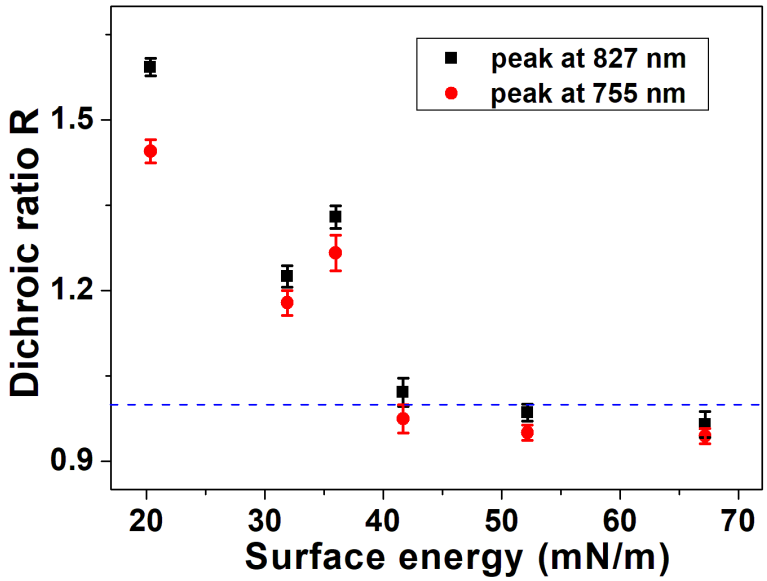

Figure S4. UV-vis dichroic ratio R (R= I_{perp}/I_{par}) of DPP2T-TT films as a function of substrate surface energy. R was calculated from the peak absorbance at 755 nm and 827 nm. The dash line indicates R=1.

Downloaded from pubs.acs.org/langd5/article-supplement/1470601/pdf/la7b02807_si_001/ by PURDUE UNIV user on 28 October 2026

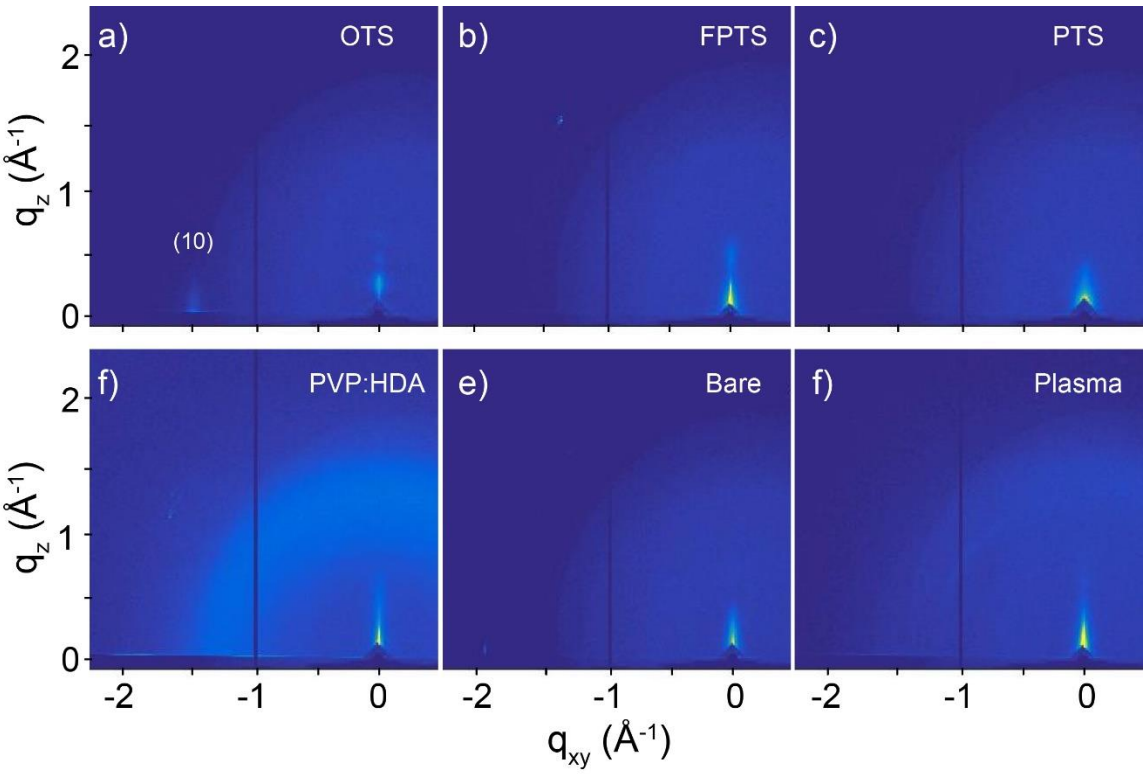

Figure S5. GIXD images of (a) OTS, (b) FPTS, (c) PTS, (c) PVP:HDA, (e) bare and (f) plasma treated Si substrate before coating the polymer semiconductor film. The diffraction of substrates demonstrated crystalline structures of the OTS monolayer, while others shown the amorphous packing. The OTS-SAM layer showed a peak at q_{xy}= 1.49Å, corresponding to the (10) diffraction of the hexagonal crystalline lattice.[14-15]

Downloaded from pubs.acs.org/langd5/article-supplement/1470601/pdf/la7b02807_si_001/ by PURDUE UNIV user on 28 October 2026

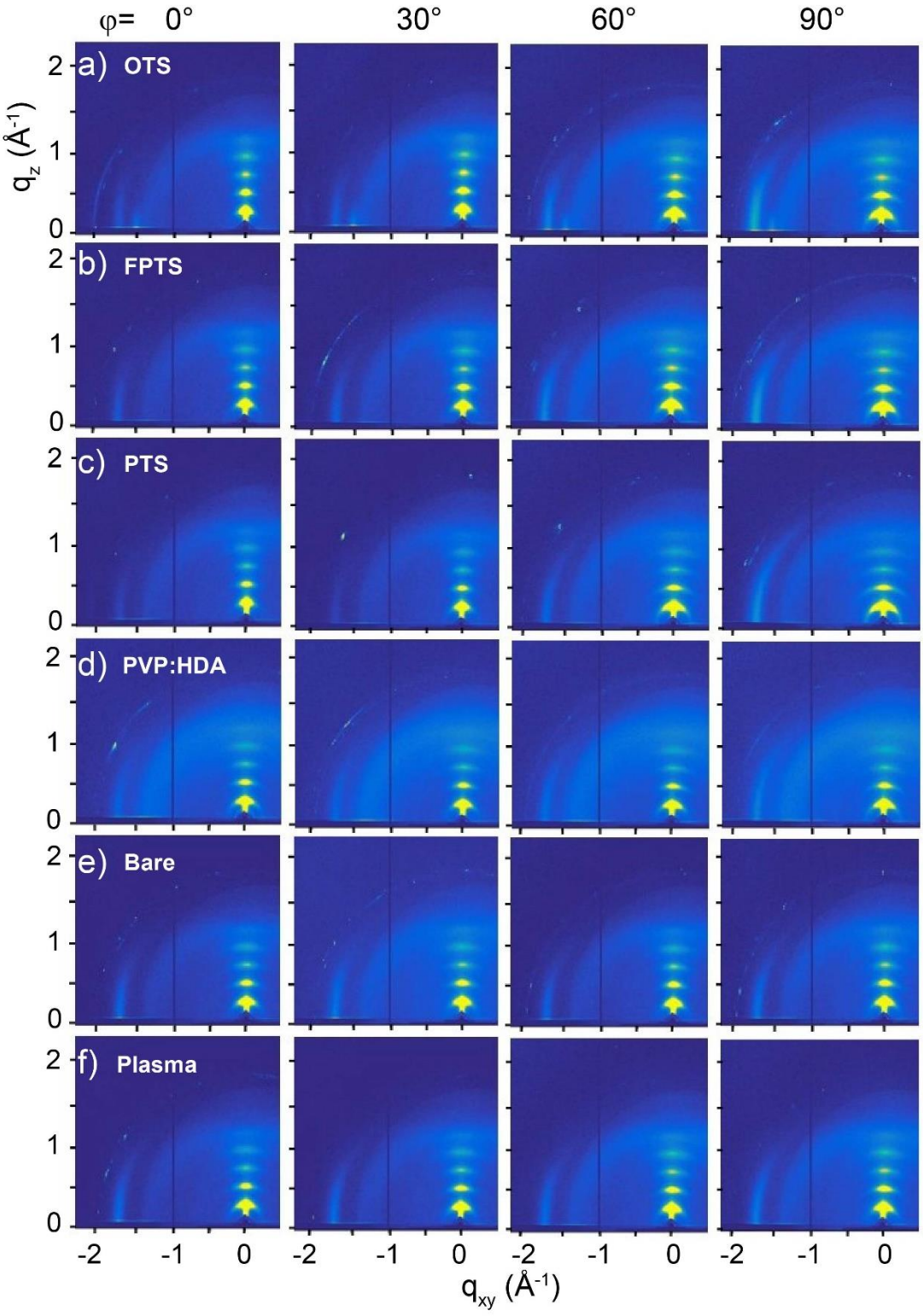

Figure S6. GIXD images of DPP2T-TT films on (a) OTS, (b) FPTS, (c) PTS, (c) PVP:HDA, (e) bare and (f) plasma treated Si substrate, at φ= 0°, 30°, 60° and 90°. The

Downloaded from pubs.acs.org/langd5/article-supplement/1470601/pdf/la7b02807_si_001/ by PURDUE UNIV user on 28 October 2026

angle φ is the in-plane rotation angle of the sample, and 0° is defined as when the coating direction is aligned with the incident beam. Note that geometrical correction was not applied to these raw images to better visualize the out-of-plane peaks. We did apply geometrical correction during analysis of the diffraction patterns.

Downloaded from pubs.acs.org/langd5/article-supplement/1470601/pdf/la7b02807_si_001/ by PURDUE UNIV user on 28 October 2026

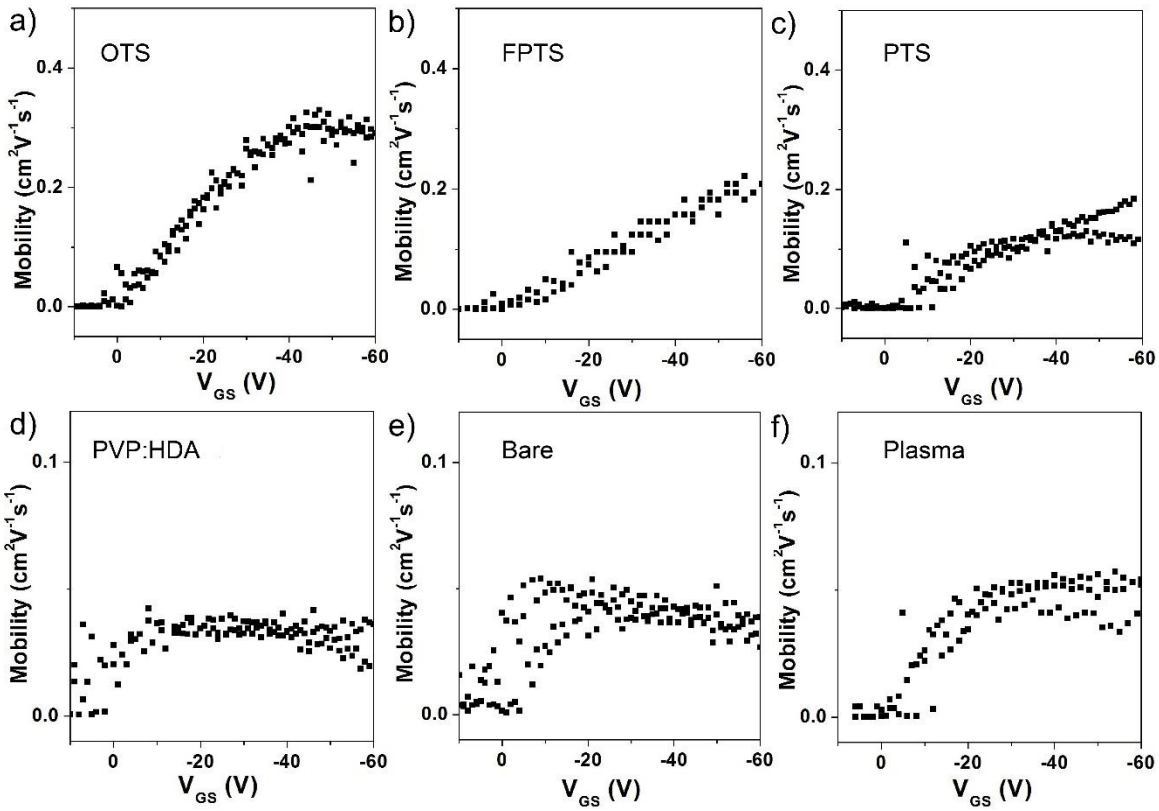

Figure S7. V_{GS} dependent apparent mobilities of DPP2T-TT OFETs with TGTC configuration in the saturation regime. The semiconducting layers were deposited on (a) OTS, (b) FPTS, (c) PTS, (d) PVP:HDA, (e) bare and (f) plasma treated SiO_2 substrates. V_{DS}= -60 V; the mobility is calculated per 2V for forward and reverse scanning.

Downloaded from pubs.acs.org/langd5/article-supplement/1470601/pdf/la7b02807_si_001/ by PURDUE UNIV user on 28 October 2026

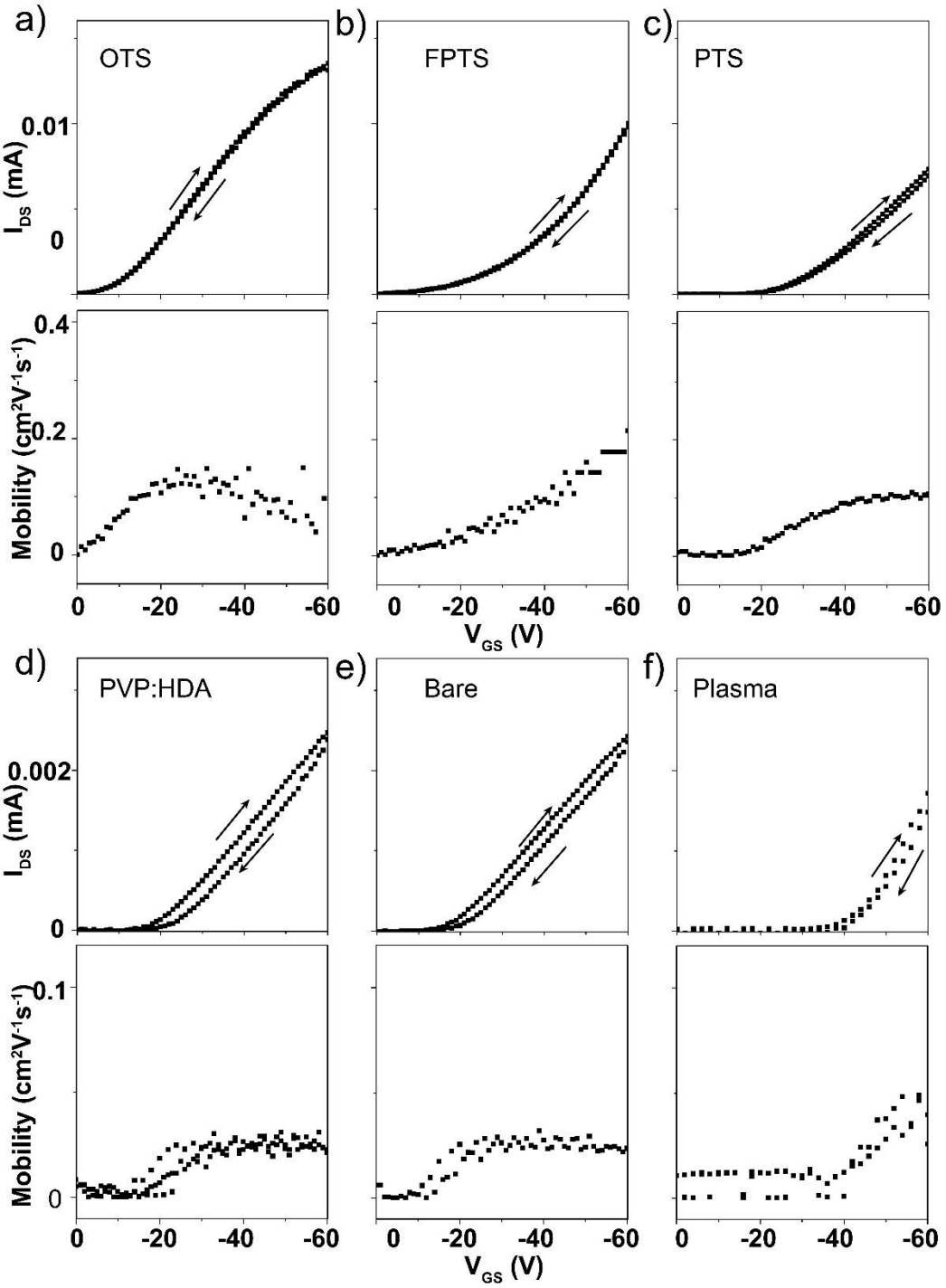

Figure S8. Transfer curves (Top) and V_{GS} dependent apparent mobilities (bottom) of DPP2T-TT TGTC OFETs in the linear regime, obtained at V_{DS}= −10 V. The semiconducting layers were deposited on (a) OTS, (b) FPTS, (c) PTS, (d) PVP:HDA, (e) bare and (f) plasma treated SiO_2 substrates.

Downloaded from pubs.acs.org/langd5/article-supplement/1470601/pdf/la7b02807_si_001/ by PURDUE UNIV user on 28 October 2026

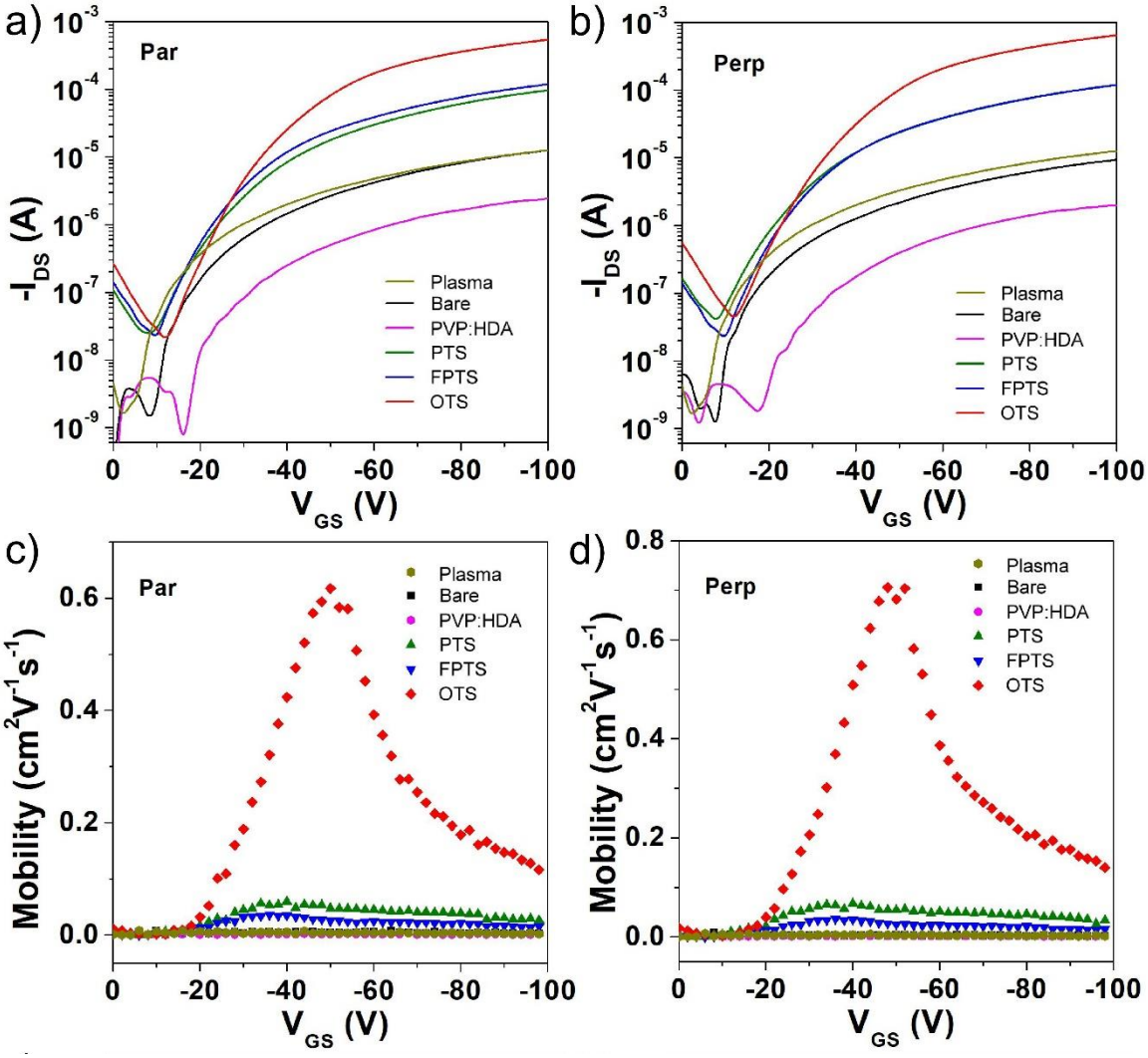

Figure S9. (a, b) Transfer curves and (c, d) mobility as a function of gate voltage for DPP2T-TT OFETs with BGTC configuration, in the saturation regime with V_{DS}= −100 V for the measurements. 'Par' and 'Perp' denote the case when the channel is parallel and perpendicular to the coating direction, respectively.

Downloaded from pubs.acs.org/langd5/article-supplement/1470601/pdf/la7b02807_si_001/ by PURDUE UNIV user on 28 October 2026

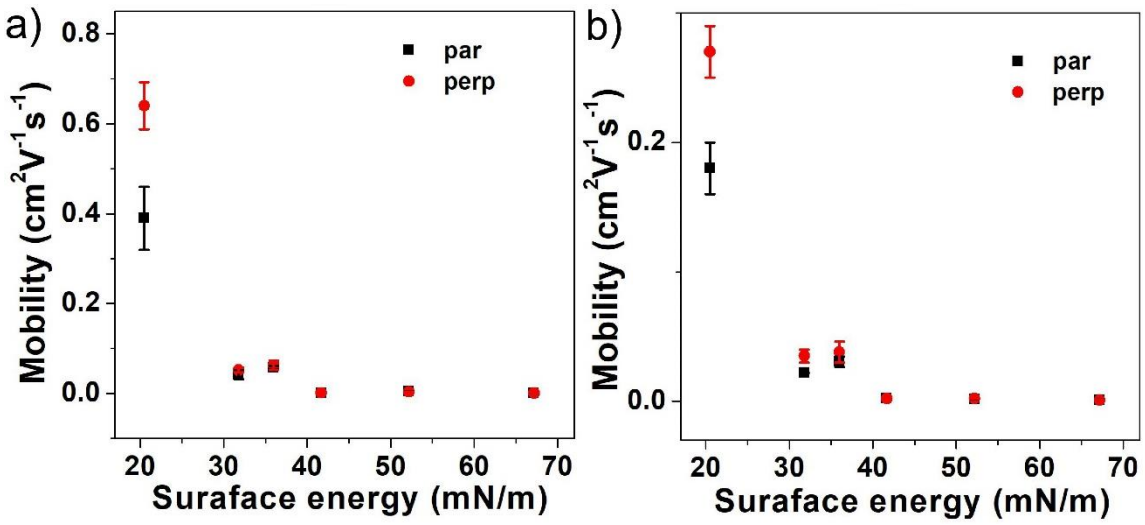

Figure S10. Apparent mobilities of BGTC OFETs as a function of surface energy. The mobility was calculated in the saturation regime in the (a) low ($0<|V_{GS}|<60$ V) and (b) high gate voltage ($60<|V_{GS}|<100$ V) regions.

Downloaded from pubs.acs.org/langd5/article-supplement/1470601/pdf/la7b02807_si_001/ by PURDUE UNIV user on 28 October 2026

Table S3. Summary of device characteristics for DPP2T-TT OFETs with TGTC and BGTC structure based on DPP2T-TT films on various substrate.

Device structure	Substrate	Surface energy (mN/m)	Channel length direction to coating	Mobility ($cm^2V^{-1}s^{-1}$)		V_{th} (V)	Log (I_{on}/I_{off})
				Low V_{GS}	High V_{GS}		
TGTC	OTS	20.5±1.4	Par	0.22±0.06		-14.5±5.4	4.7±0.9
			Perp	0.29±0.08		-15.1±3.5	4.8±0.2
	FPTS	31.8±1.5	Par	0.09±0.04		-10.6±3.2	4.1±0.3
			Perp	0.18±0.04		-12.5±1.5	4.2±0.2
	PTS	36.0±1.6	Par	0.08±0.03		-5.2±2.4	4.1±0.1
			Perp	0.14±0.02		-7.5±3.1	4.2±0.5
	PVP:HDA	41.7±1.2	Par	0.03±0.001		9.0±1.0	4.2±0.5
			Perp	0.04±0.004		-8.3±3.8	3.9±0.6
	Bare	52.2±1.0	Par	0.05±0.010		-5.4±4.5	3.8±0.6
			Perp	0.04±0.002		-7.3±5.9	5.2±0.1
	Plasma	67.2±2.4	Par	0.04±0.006		-9.0±1.1	4.2±0.2
			Perp	0.05±0.003		-12.0±0.8	4.3±0.1
BGTC	OTS	20.5±1.4	Par	0.49±0.07	0.16±0.02	-18.3±2.0	3.5±0.6
			Perp	0.74±0.02	0.18±0.01	-20.1±0.2	4.3±0.2
	FPTS	31.8±1.5	Par	0.04±0.003	0.02±0.003	-15.0±3.1	4.0±0.8
			Perp	0.05±0.001	0.03±0.005	-14.5±1.6	3.6±0.3
	PTS	36.0±1.6	Par	0.06±0.004	0.03±0.004	-21.0±2.5	3.8±0.8
			Perp	0.07±0.008	0.04±0.008	-18.0±1.0	3.6±0.3
	PVP:HDA	41.7±1.2	Par	0.001±0.0002	0.002±0.0002	-13.0±2.0	2.9±0.5
			Perp	0.001±0.0003	0.002±0.0003	-17.5±2.5	3.2±0.3
	Bare	52.2±1.0	Par	0.005±0.0002	0.004±0.0002	-13.5±1.5	3.1±0.4
			Perp	0.004±0.0001	0.006±0.0001	-9.0±1.0	3.2±0.2
	Plasma	67.2±2.4	Par	0.005±0.0002	0.004±0.0002	-15.5±2.5	3.5±0.4
			Perp	0.004±0.0001	0.005±0.0003	-11.0±3.7	3.1±0.5

Downloaded from pubs.acs.org/langd5/article-supplement/1470601/pdf/la7b02807_si_001/ by PURDUE UNIV user on 28 October 2026

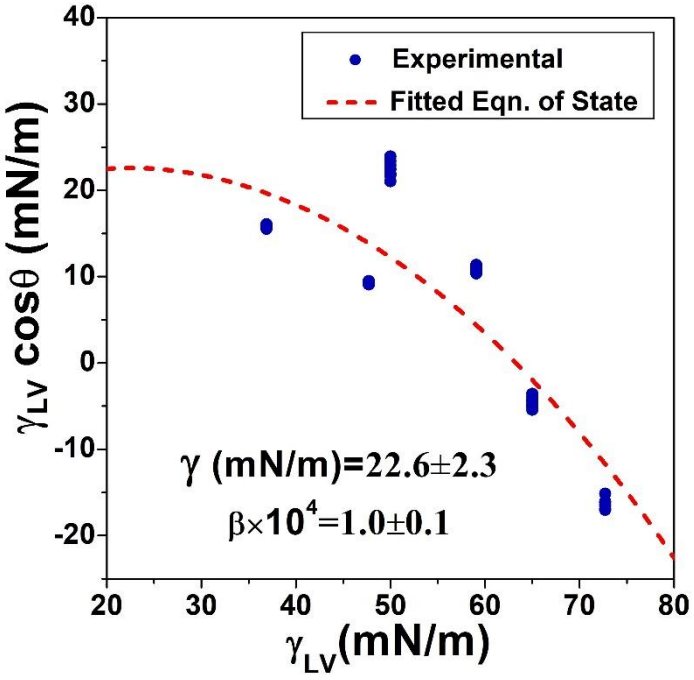

Figure S11. Determination of DPP2T-TT surface energy via the equation of state approach. The plot shown is the $\gamma_{LV} \times \cos\theta$ vs. γ_{LV} plot comparing experimental data and best-fitted curve obtained from the equation of state.

Downloaded from pubs.acs.org/langd5/article-supplement/1470601/pdf/la7b02807_si_001/ by PURDUE UNIV user on 28 October 2026

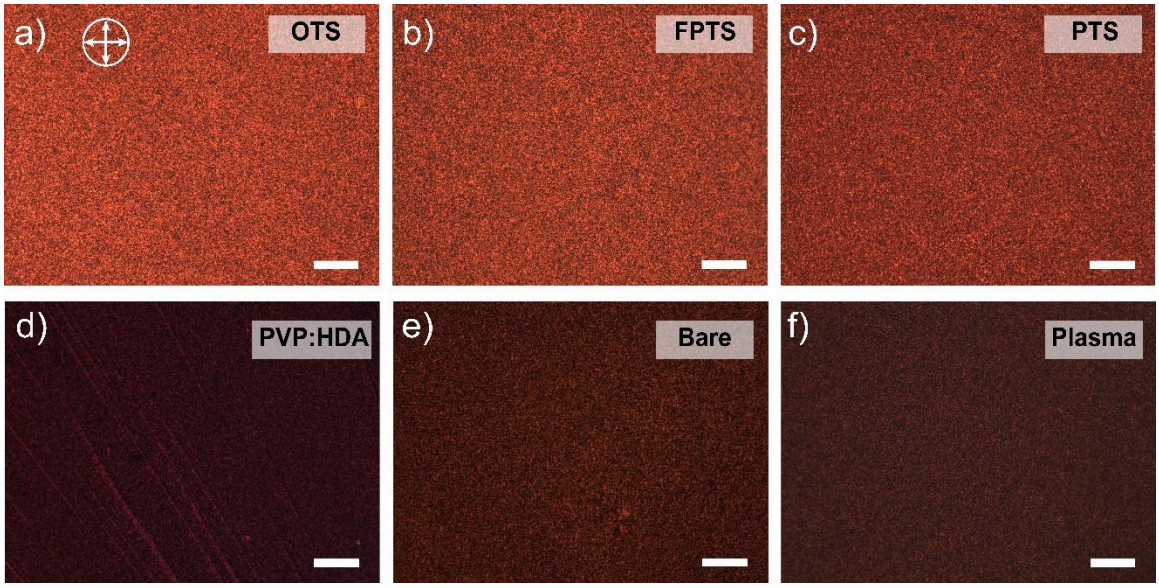

Figure S12. C-POM images for spin-coated DPP2T-TT thin films on (a) OTS, (b) FPTS, (c) PTS, (d) PVP:HDA, (e) bare and (f) plasma treated substrate, taken at the same exposure time. All scale bars are 100 μm.

Downloaded from pubs.acs.org/langd5/article-supplement/1470601/pdf/la7b02807_si_001/ by PURDUE UNIV user on 28 October 2026

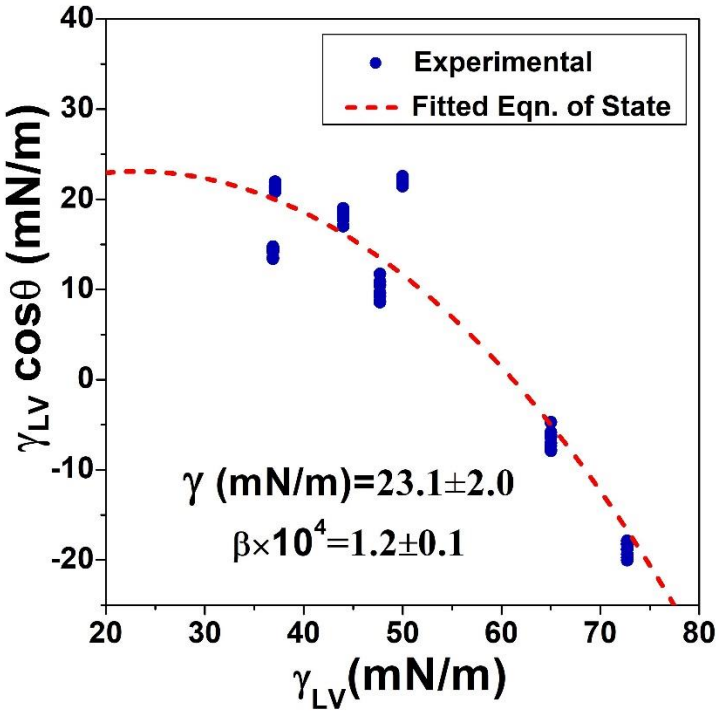

Figure S13. Determination of PII-2T surface energy via the equation of state approach. The plot shown is the $\gamma_{LV} \times \cos\theta$ vs. γ_{LV} plot comparing experimental data and best-fitted curve obtained from the equation of state.

Downloaded from pubs.acs.org/langd5/article-supplement/1470601/pdf/la7b02807_si_001/ by PURDUE UNIV user on 28 October 2026

References

1. Young, T., An Essay on the Cohesion of Fluids. *Philosophical Transactions of the Royal Society of London* **1805,** *95*, 65-87.
2. Kwok, D. Y.; Neumann, A. W., Contact angle measurement and contact angle interpretation. *Adv. Colloid Interface Sci.* **1999,** *81*, 167-249.
3. Fordham, S., On the Calculation of surface tension from measurements of pendant drops. *Proc. R. Soc. London Ser. A-Math. Phys. Eng. Sci.* **1948,** *194*, 1-16.
4. Li, D.; Neumann, A. W., Contact angles on hydrophobic solid surfaces and their interpretation. *J. Colloid Interface Sci.* **1992,** *148*, 190-200.
5. Li, D.; Xie, M.; Neumann, A. W., Vapour adsorption and contact angles on hydrophobic solid surfaces. *Colloid. Polym. Sci.* **1993,** *271*, 573-580.
6. Kwok, D. Y.; Li, D.; Neumann, A. W., Fowkes' surface tension component approach revisited. *Colloid Surf. A-Physicochem. Eng. Asp.* **1994,** *89*, 181-191.
7. Neumann, A. W.; Good, R. J.; Hope, C. J.; Sejpal, M., An equation-of-state approach to determine surface tensions of low-energy solids from contact angles. *J. Colloid Interface Sci.* **1974,** *49*, 291-304.
8. Israelachvili, J. N., *Intermolecular and surface forces*. Academic press: 2015.
9. Mason, R. L.; Gunst, R. F.; Hess, J. L., *Statistical design and analysis of experiments: with applications to engineering and science*. John Wiley & Sons: 2003; Vol. 474.
10. Cheng, P.; Li, D.; Boruvka, L.; Rotenberg, Y.; Neumann, A. W., Automation of axisymmetric drop shape analysis for measurements of interfacial tensions and contact angles. *Colloid Surf.* **1990,** *43*, 151-167.
11. Perry, R. H.; Green, D. W., *Perry's chemical engineers' handbook*. McGraw-Hill Professional: 1999.

Downloaded from pubs.acs.org/langd5/article-supplement/1470601/pdf/la7b02807_si_001/ by PURDUE UNIV user on 28 October 2026

12. Neumann, A. W., Contact angles and their temperature dependence: thermodynamic status, measurement, interpretation and application. *Adv. Colloid Interface Sci.* **1974,** *4*, 105-191.

13. Le Berre, M.; Chen, Y.; Baigl, D., From convective assembly to Landau-Levich deposition of multilayered phospholipid films of controlled thickness. *Langmuir* **2009,** *25*, 2554-2557.

14. Lee, H. S.; Kim, D. H.; Cho, J. H.; Hwang, M.; Jang, Y.; Cho, K., Effect of the phase states of self-assembled monolayers on pentacene growth and thin-film transistor characteristics. *J. Am. Chem. Soc.* **2008,** *130*, 10556-10564.

15. Hiszpanski, A. M.; Loo, Y.-L., Directing the film structure of organic semiconductors via post-deposition processing for transistor and solar cell applications. *Energy Environ. Sci.* **2014,** *7*, 592-608.

Downloaded from pubs.acs.org/langd5/article-supplement/1470601/pdf/la7b02807_si_001/ by PURDUE UNIV user on 28 October 2026